Effects of degeneracy removal on optical and magneto-optical properties of 3d ferromagnetic metals

1990 J. Phys.: Condens. Matter 2 6137

(http://iopscience.iop.org/0953-8984/2/28/005)

J. Phys.: Condens. Matter **2** (1990) 6137–6152. Printed in the UK

Effects of degeneracy removal on optical and magneto-optical properties of 3d ferromagnetic metals

S V Halilov and Yu A Uspenskii
Lebedev Physical Institute, 117924, Moscow, USSR

Received 7 March 1989, in final form 22 January 1990

Abstract. We consider the effects of degeneracy removal due to magnetism and spin–orbit coupling on the optical and magneto-optical properties of Fe, Co and Ni. Both analytical and numerical calculations were carried out in order to investigate the frequency dependence of the conductivity tensor in the presence of spin–polarisation and spin–orbit coupling. Anomalies of the tensor are predicted in the infrared region at energies of the order of the spin–orbit splitting. A universal explanation is proposed for these anomalies. This is that paired singularities of the tensor components, at energies of the order of the d-band give information about the exchange splitting of the d-band. The obtained results are in accordance with optical, magneto-optical and photoemission measurements.

1. Introduction

Optical measurements are widely used for the investigation of the electron structure of solids. However, the interpretation of optical curves turns out to be very complicated in many cases. For magnetic materials where a spin degeneracy is removed, the interpretation is especially difficult. Probably the best approach is the first-principles calculation used as the basis for the explanation of optical properties. Earlier such calculations have been carried out for some ferromagnetic metals [1–5]. They reproduced the experimental curves rather well and allowed identification of some features of the optical curves. However, this work did not pay much attention to the specific manifestations of the magnetic effect on optics. This is not surprising because optical conductivity is in the first approximation just the sum of the conductivities of electrons with different spin projections and therefore depends on the spin structure rather weakly. On the other hand the magneto-optical effects of Faraday, Kerr, etc, which disappear in the absence of a magnetic field (both internal and external), have a strong dependence on spin ordering. At present there are a few first-principles calculations of magneto-optical effects [1–3] in satisfactory agreement with experimental data but the detailed interpretation of the magneto-optics is nearly absent.

In this paper we present our relativistic and non-relativistic LMTO calculations of the conductivity tensor $\sigma_{\alpha\beta}(\omega)$ for ferromagnets Fe, Co (FCC, HCP), Ni and concentrate on the manifestations of the spin–polarisation and relativistic effects. On this basis we construct simple models describing the main features of $\sigma_{\alpha\beta}(\omega)$ in the infrared, visible and ultraviolet spectral regions. Such unified numerical and analytical consideration allows identification of some features of the optical and magneto-optical curves with

0953-8984/90/286137 + 16 $03.50

fundamental band parameters namely the spin–orbit (SO) and exchange splitting and the d-band width. Then these parameters can be extracted by the appropriate interpretation from the optical and magneto-optical measurements.

Our paper is organised as follows. In section 2 we give a short review of the theoretical results on the optics and magneto-optics. Section 3 contains the numerical results for the visible and ultraviolet regions and our interpretation of the corresponding features of $\sigma_{\alpha\beta}(\omega)$ based on a simple model of the band structure. It is found that the estimates of the d-band width and the exchange splitting extracted from the magneto-optics are in good agreement with photoemission data. Section 4 is devoted to the infrared region. Previously we have considered the specific features of the infrared optics in non-relativistic and also partly in relativistic cases [6]. Our analysis shows that in this region a non-zero interband contribution to $\sigma_{\alpha\beta}(\omega)$ occurs only when at least one of three standard situations takes place. For each situation we derive an analytical expression for $\sigma_{\alpha\beta}(\omega)$ using the $\boldsymbol{k}\cdot\boldsymbol{p}$ perturbation theory. The numerical investigation confirms this analysis and allows identification of the situation for each metal. Finally in section 5 we give concluding remarks and a summary.

2. Frequency-dependent conductivity tensor

In the random-phase approximation and without local-field corrections the real and imaginary parts of the conductivity tensor are given by the following expressions based on Kubo's [7] formula for linear response:

$$\begin{aligned}\operatorname{Re}\sigma_{\alpha\beta}(\omega) = {} & \frac{\pi e^2}{2}\delta(\omega)\sum_{k\lambda}\delta(E_{k\lambda}-E_{\mathrm{F}})\operatorname{Re}[j_\alpha^{\lambda\lambda}(\boldsymbol{k})j_\beta^{\lambda\lambda}(\boldsymbol{k})] \\ & + \hbar e^2\sum_{k\lambda\neq\lambda'} f_{k\lambda}(1-f_{k\lambda})\left(\operatorname{Im}[j_\alpha^{\lambda'\lambda}(\boldsymbol{k})j_\beta^{\lambda'\lambda}(\boldsymbol{k})]P\frac{1}{\hbar^2\omega^2-E_{\lambda\lambda'}^2(\boldsymbol{k})}\right. \\ & \left. + \operatorname{Re}[j_\alpha^{\lambda'\lambda}(\boldsymbol{k})j_\beta^{\lambda'\lambda}(\boldsymbol{k})]\frac{\pi\delta[\hbar\omega-E_{\lambda\lambda'}(\boldsymbol{k})]}{2\hbar\omega}\right) \qquad (1)\end{aligned}$$

$$\begin{aligned}\operatorname{Im}\sigma_{\alpha\beta}(\omega) = {} & \frac{e^2}{\omega}\sum_{k\lambda}\delta(E_{k\lambda}-E_{\mathrm{F}})\operatorname{Re}[j_\alpha^{\lambda\lambda}(\boldsymbol{k})j_\beta^{\lambda\lambda}(\boldsymbol{k})] + \hbar e^2\sum_{k\lambda\neq\lambda'} f_{k\lambda}(1-f_{k\lambda}) \\ & \times\left(\operatorname{Re}[j_\alpha^{\lambda'\lambda}(\boldsymbol{k})j_\beta^{\lambda'\lambda}(\boldsymbol{k})]P\frac{1}{\hbar^2\omega^2-E_{\lambda\lambda'}^2(\boldsymbol{k})}\frac{E_{\lambda\lambda'}(\boldsymbol{k})}{\hbar\omega}\right. \\ & \left. + \operatorname{Im}[j_{\alpha\alpha}^{\lambda'\lambda}(\boldsymbol{k})j_\beta^{\lambda'\lambda}(\boldsymbol{k})]\frac{\pi\delta[\hbar\omega-E_{\lambda\lambda'}(\boldsymbol{k})]}{2\hbar\omega}\right) \qquad (2)\end{aligned}$$

where $E_{\lambda\lambda'}(\boldsymbol{k}) = E_{k\lambda} - E_{k\lambda'}$ and $f_{k\lambda'}$, $E_{k\lambda}$, $|k\lambda\rangle$ are the occupation number, the energy and the one-electron wavefunction in the λ band, respectively. Equations (1) and (2) correspond to the zero limit of the relaxation frequency of electron states. In this limit the intraband contributions to the conductivity tensor are described by the first terms in equations (1), (2). The other terms come from the interband transitions. Further we shall take into account relativistic effects in v^2/c^2 and shall use the wavefunction obeying

Kohn–Sham–Foldy–Wouthuysen-like equation in order to calculate the matrix elements:

$$j_{\alpha\alpha}^{\lambda'\lambda}(\boldsymbol{k}) \equiv (1/m)\langle \boldsymbol{k}\lambda'|p_\alpha + (\hbar/4mc^2)[\boldsymbol{\sigma} \times \boldsymbol{\nabla} v_{\text{eff}}]_\alpha|\boldsymbol{k}\lambda\rangle \tag{3}$$

where the second term of order $\langle \boldsymbol{k}\lambda'|p_\alpha|\boldsymbol{k}\lambda\rangle E_{\lambda\lambda'}(\boldsymbol{k})/4mc^2$ can be omitted. In fact it is sufficient to calculate either Re $\sigma_{\alpha\beta}(\omega)$ or Im $\sigma_{\alpha\beta}(\omega)$ (e.g. Re $\sigma_{\alpha\alpha}$ or Im $\sigma_{\alpha\beta}(\alpha \neq \beta)$) since other quantities can be obtained from the Kramers–Kronig relations.

The tensor $\sigma_{\alpha\beta}(\omega)$ has the form required by the magnetic space group. The symmetric restrictions imposed by the given magnetic space group are the same as those imposed by its Laue group (see [8]). The Laue group of a group is defined as the group obtained from the given group by replacing every translation by the identity, and replacing every improper rotation by its proper counterpart. If the tensor is subjected to the elements of Laue group, then the next form of $\sigma_{\alpha\beta}(\omega)$ is obtained for the magnetisation orientations $\boldsymbol{M} \parallel [001]$ and $\boldsymbol{M} \parallel [110]$:

$$\sigma_{\alpha\beta}^{[001]} = \begin{bmatrix} \sigma_{xx} & \sigma_{xy} & 0 \\ -\sigma_{xy} & \sigma_{xx} & 0 \\ 0 & 0 & \sigma_{zz} \end{bmatrix} \qquad \sigma_{\alpha\beta}^{[110]} = \begin{bmatrix} \sigma_{xx} & \sigma_{xy} & \sigma_{xz} \\ \sigma_{xy} & \sigma_{xx} & -\sigma_{xy} \\ -\sigma_{xz} & \sigma_{xz} & \sigma_{zz} \end{bmatrix}. \tag{4}$$

As a result at this point we come straightforwardly to the conclusion that the components Im $\sigma_{\alpha\beta}(\alpha \neq \beta)$, antisymmetric in indices α, β, are

$$\text{Im}\,\sigma_{\alpha\beta}(\omega) = \frac{\pi e^2}{2\omega} \sum_{\boldsymbol{k}\lambda\lambda'} \delta[\hbar\omega - E_{\lambda\lambda'}(\boldsymbol{k})] f_{\boldsymbol{k}\lambda}(1 - f_{\boldsymbol{k}\lambda'})\,\text{Im}[j_\alpha^{\lambda\lambda'}(\boldsymbol{k}) j_\beta^{\lambda'\lambda}(\boldsymbol{k})] \tag{5}$$

and the symmetric components Re $\sigma_{\alpha\beta}$ are

$$\text{Re}\,\sigma_{\alpha\beta}(\omega) = \frac{\pi e^2}{2}\,\delta(\omega) \sum_{\boldsymbol{k}\lambda} \delta(E_{\boldsymbol{k}\lambda} - E_{\text{F}})\,\text{Re}[j_\alpha^{\lambda\lambda}(\boldsymbol{k}) j_\beta^{\lambda\lambda}(\boldsymbol{k})]$$

$$+ \frac{\pi e^2}{2\omega} \sum_{\boldsymbol{k}\lambda\lambda'} \delta[\hbar\omega - E_{\lambda\lambda'}(\boldsymbol{k})] f_{\boldsymbol{k}\lambda}(1 - f_{\boldsymbol{k}\lambda'})\,\text{Re}(j_\alpha^{\lambda\lambda'}(\boldsymbol{k}) j_\beta^{\lambda'\lambda}(\boldsymbol{k})]. \tag{6}$$

The symmetric components of $\sigma_{\alpha\beta}$ are even in $\boldsymbol{M}$ and the antisymmetric components are odd in $\boldsymbol{M}$. More precisely, symmetric and antisymmetric components of $\sigma_{\alpha\beta}$ are proportional to even or odd powers of the parameter $\gamma \equiv [(n_\uparrow - n_\downarrow)/n_\uparrow](\overline{2\xi}/\overline{\Delta E_{\lambda\lambda'}})$, respectively, where $2\overline{\xi}$ is the mean value of the SO splitting, and $\overline{\Delta E_{\lambda\lambda'}}$ is $E_{\lambda\lambda'}$ averaged over the bands with the same spin projections. Assuming that $2\overline{\xi} \simeq 0.2$ eV, $\overline{\Delta E_{\lambda\lambda'}} \simeq W_{\text{d}}/5 \simeq 1$ eV (W_{d} is the d-band width) and $(n_\uparrow - n_\downarrow)/n_\uparrow \simeq \frac{1}{3}$, we find that $\gamma \simeq \frac{1}{15}$. Therefore we have the following typical orders of magnitude: $\sigma_{xy}^{[001]} \sim \sigma_{xz}^{[110]} \sim \gamma\sigma_{\alpha\alpha}$ and $\sigma_{xy}^{[110]} \sim \gamma^2\sigma_{\alpha\alpha}$, in accordance with the experimental data [9–11].

Conventional optics are determined mainly by the diagonal components of the conductivity $\sigma_{\alpha\alpha}(\omega)$. On the contrary, the antisymmetric non-diagonal components of $\sigma_{\alpha\beta}$ are the source of the Faraday effect. The angle of rotation of the light polarisation is given by the expression

$$\alpha_{\text{F}} = (\omega d/2c)\,\text{Re}[n^{\text{r}} - n^{\text{l}}] \qquad n^{\text{r,l}} = \sqrt{1 + 4\pi i\sigma^{\text{r,l}}(\omega)/\omega} \tag{7}$$

where d is the thickness of a sample and c is the velocity of light. For $\boldsymbol{M} \parallel [001]$ the right and left conductivities are

$$\sigma^{\text{r,l}}(\omega) = \sigma_{xx}(\omega) \pm i\sigma_{xy}(\omega). \tag{8}$$

Thus α_{F} turns out to be proportional to $\sigma_{xy}(\omega)$.

Further we shall be interested in the components of the tensor that describe the light dissipation Q. The expressions for these components depend on the magnetisation orientation and are contained in the following expression for Q:

$$Q = (1/4\pi)\langle E\,\partial D/\partial t\rangle_t = \tfrac{1}{2}\,\mathrm{Re}[\sigma_{\alpha\beta}E^*_\alpha E_\beta] \tag{9}$$

where $\langle\ldots\rangle_t$ denote an average over time. For instance, as is easily seen from equations (4) and (9), the light dissipation is described by Re $\sigma_{\alpha\alpha}$ and Im σ_{xy} for $\boldsymbol{M}\parallel[001]$ and by Re $\sigma_{\alpha\alpha}$, Re σ_{xy} and Im σ_{xz} for $\boldsymbol{M}\parallel[110]$.

For the analysis of $\sigma_{xy}(\omega)$ it is convenient to use the perturbative expression derived by Argyres [12]:

$$\mathrm{Im}\,\sigma_{xy}(\omega) = \frac{\pi e^2}{\hbar\omega m^2}\sum_{km'\neq m}\{F^{xy}_{m'm\uparrow}(\boldsymbol{k})f_{km'\uparrow}(1-f_{km\uparrow})\,\delta[\hbar\omega - E_{mm'\uparrow}(\boldsymbol{k})]$$
$$- F^{xy}_{m'm\downarrow}(\boldsymbol{k})f_{km'\downarrow}(1-f_{km\downarrow})\delta[\hbar\omega - E_{mm'\downarrow}(\boldsymbol{k})]\} \tag{10}$$

$$F^{xy}_{m'm\sigma}(\boldsymbol{k}) \equiv 2\mathrm{i}\sum_l{}'\left(\frac{L^{z*}_{lm'}}{E_{m'l}}p^{lm}_x p^{m'm}_y + \frac{L^z_{lm}}{E_{ml}}p^{lm'}_x p^{m'm}_y\right)_\sigma \tag{11}$$

where $L^z_{lm\sigma} \equiv \langle \boldsymbol{k}l\sigma|\xi\hat{l}_z|\boldsymbol{k}m\sigma\rangle$ ($\xi \equiv (2/rc^2)\,\partial v_{\mathrm{eff}}/\partial r$ is the radial SO parameter and $\hat{l}$ the angular momentum operator) and $|\boldsymbol{k}m\sigma\rangle$ are the non-relativistic states in bands $m\uparrow$ or $m\downarrow$. These formulae are valid in the lowest order in γ at frequencies $\omega \gg 2\bar{\xi}/\hbar$ only. The expressions appropriate for an infrared region will be derived in section 4.

3. Optics and magneto-optics in the energy region 0.5 eV $\leqslant \hbar\omega \leqslant$ 10 eV

Further details of the dynamical behaviour of $\sigma_{\alpha\beta}(\omega)$ are based on first-principles calculations. We have calculated the band structure for the ferromagnetic Fe (BCC), Co (FCC, HCP) and Ni (FCC) with $\boldsymbol{M}\parallel[001]$ using both the non-relativistic and the relativistic LMTO method [12] and the self-consistent spin-polarised potentials. The integration over $\boldsymbol{k}$ in equations (1) and (2) has been performed by the tetrahedron method with 615, 525 and 325 points in the irreducible part of the Brillouin zone (BZ) for BCC ($\frac{1}{16}$ BZ), FCC ($\frac{1}{16}$ BZ) and HCP ($\frac{1}{12}$ BZ), respectively. Other details of our calculation can be found in [14]. In figures 1–5 we present our results for Re $\sigma_{xx}(\omega)$, Im $\sigma_{xy}(\omega)$ and the available experimental data [9, 10, 15–17]. For Fe and Co the rather good accordance between the theory and the experiment is noticeable while for Ni the theoretical curves have the same shape as the experimental curve but are very broad in energy. The calculations for both FCC and HCP Co demonstrate the crystal structure dependence of the conductivity tensor. In spite of the difference in the visible region there is rather the same behaviour of the conductivity tensor in the ultraviolet for Co with a different crystal structure. The specific behaviour of the tensor in ultraviolet can be considered as a manifestation of the magnetic effect weakly depended on the crystal structure.

Because the main features of Re $\sigma_{\alpha\alpha}(\omega)$ were identified for Fe and Ni earlier [4, 5], we restrict our consideration of the optics to only two moments. Firstly, in the ferromagnetic 3D metals the spin-up d band is almost fully occupied; hence the spin-up transitions are nearly negligible in the d band and at the energies $\hbar\omega < W_{\mathrm{d}}$ the contribution Re $\sigma^{\downarrow}_{xx}(\omega)$ dominates the conductivity. Secondly, there are paired maxima at $\hbar\omega \simeq 5.3$ and 6.5 eV (Fe), $\hbar\omega \simeq 5.0$ and 6.0 eV (Co) and $\hbar\omega \simeq 5.2$ and 5.7 eV (Ni) due to the transitions $1\uparrow \rightarrow 6\uparrow$ and $1\downarrow \rightarrow 6\downarrow$ ($1\uparrow, 2\uparrow \rightarrow 11\uparrow, 12\uparrow$ and $1\downarrow, 2\downarrow \rightarrow 11\downarrow$,

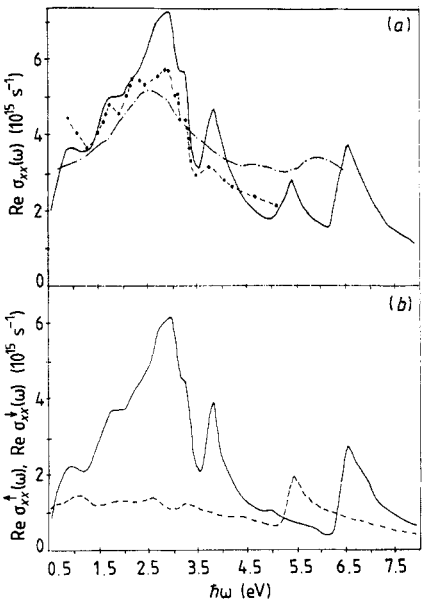

Figure 1. (*a*) Frequency dependence of Re $\sigma_{xx}(\omega)$ for Fe: - -●- -, [15]; —·—, [9]. (*b*) Spin-up Re $\sigma_{xx}^{\uparrow}(\omega)$ (– – –) and spin-down Re $\sigma_{xx}^{\downarrow}(\omega)$ (——) fractions of Re $\sigma_{xx}(\omega)$.

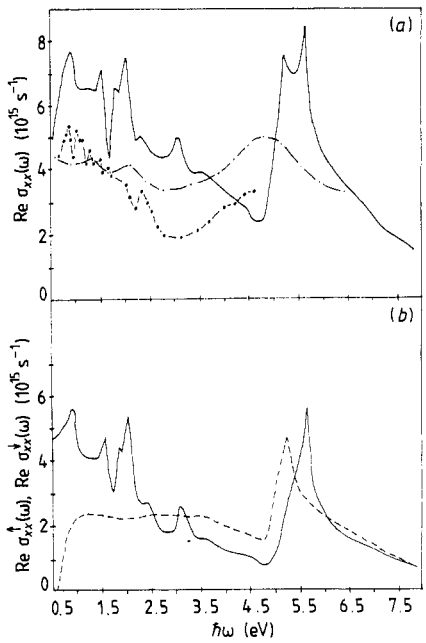

Figure 2. (*a*) Frequency dependence of Re $\sigma_{xx}(\omega)$ for Ni: - -●- -, [16]; —·—, [9]. (*b*) same as in figure 1(*b*).

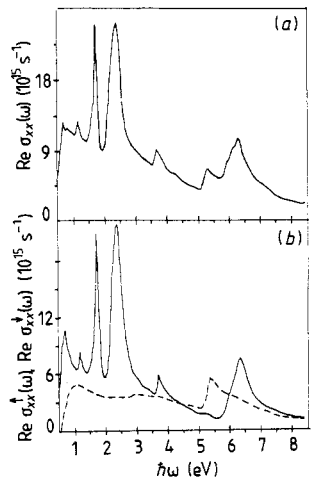

Figure 3. (*a*) Frequency dependence of Re $\sigma_{xx}(\omega)$ for Co (FCC). (*b*) Same as in figure 1(*b*).

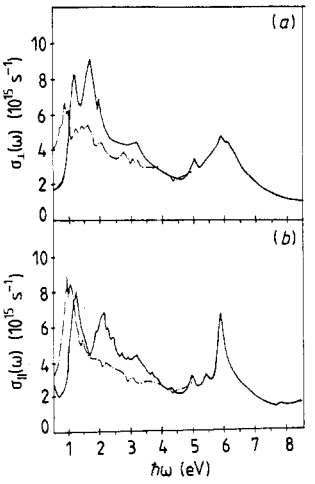

Figure 4. Frequency dependence of (*a*) $\sigma_{\perp}(\omega)$ ($\equiv \frac{1}{2}$[Re $\sigma_{xx}(\omega)$ + Re $\sigma_{yy}(\omega)$]) and (*b*) $\sigma_{\parallel}(\omega)$ ($\equiv$ Re $\sigma_{zz}(\omega)$) for Co (HCP): – – –, [17].

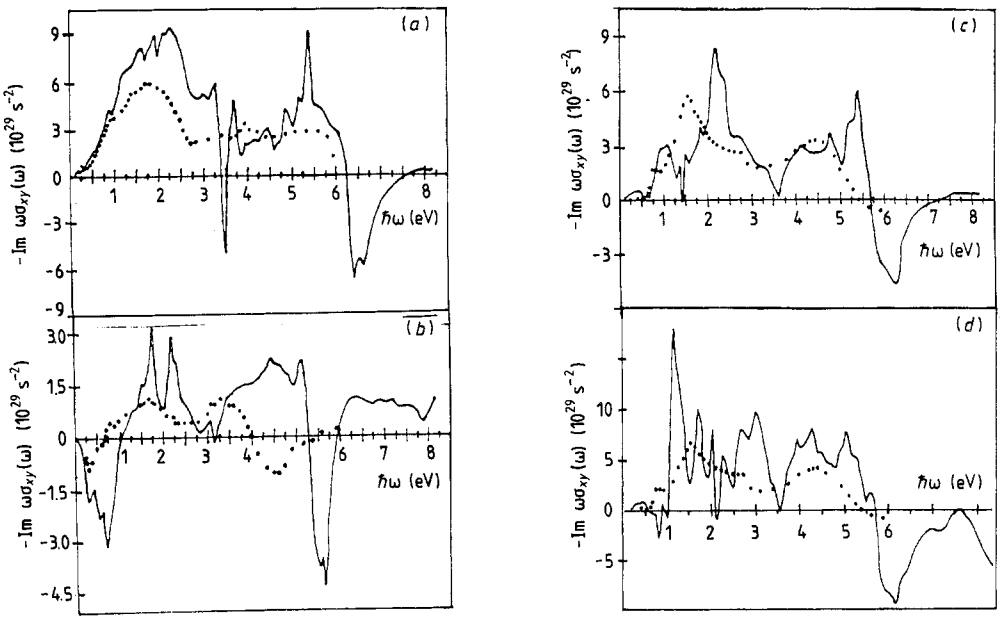

Figure 5. Frequency dependence of $-\mathrm{Im}\ \omega\sigma_{xy}(\omega)$ (*a*) for Fe, (*b*) for Ni, (*c*) for Co (FCC) and (*d*) for Co (HCP): · · ·, experimental data [9].

Table 1. The d-band width W_d for Fe, Co and Ni.

	W_d (eV)			
	Band calculation	Magneto-optics (calculated)	Magneto-optics (experimental)	Photoemission (experimental)
Fe	4.8 (Δ)	4.8	4.3 [23]	4.5 [24]
Co	4.5 (Δ)	4.5	3.9 [23]	3.8 (Δ) [25]
Ni	4.7 (L)	4.7	3.1 [23]	3.4 (L) [19]

$12\downarrow$ in the case of the HCP structure the numbers refer to band states). This situation reflects the difference in the exchange splitting for the essentially sp-like sub-bands $1\uparrow$, $1\downarrow$ and d-like sub-bands $6\uparrow$, $6\downarrow$. The mean value of the exchange splitting $2\Delta_{xc}^{d}$ of d-like sub-bands is four to five times larger than that of the exchange splitting $2\Delta_{xc}^{s}$ of the sp-like sub-bands. As a result the interband transitions $1\uparrow \rightarrow 6\uparrow$ and $1\downarrow \rightarrow 6\downarrow$ lead to the appearance of paired peaks at $\hbar\omega \simeq W_d$ mentioned above, which are separated by the magnitude of the d-band exchange splitting $2\Delta_{xc}^{d}$. The corresponding model of the band structure is schematically presented in figure 6. We believe that these paired peaks are the only feature of $\mathrm{Re}\ \sigma_{\alpha\alpha}(\omega)$ that gives the opportunity to get the d-band exchange splitting from the usual optical measurements.

It should be noted that the magneto-optical data provide more extensive information about the magnetic and SO effects in ferromagnets. As is seen from figure 5, $\mathrm{Im}\ \sigma_{xy}(\omega)$ changes its sign in the ultraviolet region. It is typical for all considered metals. The

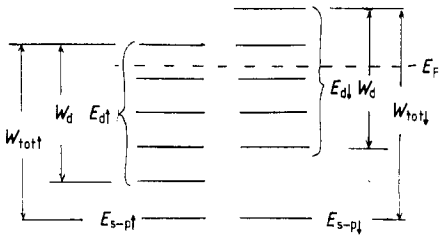

Figure 6. Band model presented schematically, allowing the treatment of the behaviour of a conductivity tensor via frequency in the visible and ultraviolet regions.

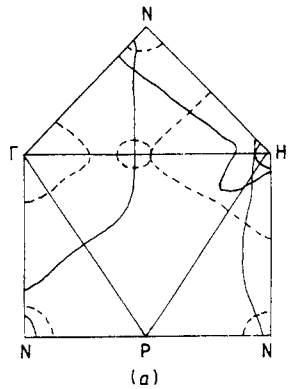

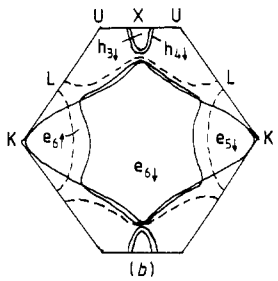

Figure 7. Cross section of the Fermi surface (*a*) of Fe and (*b*) of Ni: – – –, spin-up sheets; ——, spin-down sheets. The main contribution to $\sigma_{\alpha\beta}(\omega)$ is at $\hbar\omega \simeq 2\bar{\xi}$ in Fe and at $\hbar\omega \simeq 2\sqrt{\Delta^2 + \bar{\xi}^2}$ in Ni in the following regions: (*a*) in Fe, the easily seen intersections of sheets with the opposite spins; (*b*) in Ni, the observation of two band sheets quasi-parallel to each other.

resemblance of the theoretical and experimental curves to each other is also obvious. To explain the frequency dependence of Im $\sigma_{xy}(\omega)$ we turn to equations (10) and (11). At $2\bar{\xi} \ll \hbar\omega < W_d$ the m, m' states and most of l states in equations (10) and (11) are essentially d-like state. The spin projection exerts a very small influence on the energy differences $E_{mm'\sigma}$, $E_{ml\sigma}$ and $E_{m'l\sigma}$ and on the value of the matrix elements $L^z_{ml\sigma}$, $L^z_{m'l\sigma}$ (m, m', l belong to the d-like sub-bands). This conclusion is supported by numerical estimates of the difference of the matrix elements with opposite spin projections which is no more than 5% on average. Hence, we can safely suppose that $F^{xy}_{m'm\uparrow} \simeq F^{xy}_{m'm\downarrow} \equiv F^{xy}_{d'd}$ and we may simplify equation (10), writing it in the following form:

$$\text{Im}\,\sigma_{xy}(\omega) = \frac{\pi e^2}{\hbar\omega m^2} \sum_{kd' \neq d} F^{xy}_{d'd}(\boldsymbol{k})\delta[\hbar\omega - E_{d'd}(\boldsymbol{k})][f_{kd'\uparrow}(1 - f_{kd\uparrow}) - f_{kd'\downarrow}(1 - f_{kd\downarrow})]. \qquad (12)$$

It is obvious that the factors $\delta[\hbar\omega - E_{d'd}(\boldsymbol{k})]f_{kd'\sigma}(1 - f_{kd\sigma})$ in equation (12) are the same as those in equation (6) for the diagonal component Re $\sigma^s_{xx}(\omega)$, $s = \uparrow, \downarrow$. Thus we can

Table 2. The mean d-band exchange splitting of Fe, Co and Ni. $2\Delta^{s}_{xc}$ is the mean exchange splitting of sp-type band ($2\Delta^{s}_{xc} \ll 2\Delta^{d}_{xc}$).

	Mean d-band exchange splitting (eV)			
	Band calculation	Magneto-optics (calculated)	Magneto-optics (experimental)	Photoemission (experimental)
Fe	1.8 (Γ'_{25})	$1.4 + 2\Delta^{s}_{xc}$	$1.8 + 2\Delta^{s}_{xc}$ [18]	2.0 [26] 1.5 (P_4) [27]
Co	1.4 (Δ)	$1.2 + 2\Delta^{s}_{xc}$	$1.4 + 2\Delta^{s}_{xc}$ [18]	1.1 [27]
Ni	0.65 (L_3)	$0.5 + 2\Delta^{s}_{xc}$	$0.9 + 2\Delta^{s}_{xc}$ [18]	0.33 (Δ) [28] 0.30 (L_3) [18]

assume that at $\hbar\omega < W_d$ the quantity Im $\sigma_{xy}(\omega)$ can be approximately described by the difference $\mathrm{Re}[\sigma^{\uparrow}_{xx}(\omega) - \sigma^{\downarrow}_{xx}(\omega)]$. This assumption can be also justified by comparing the calculated curves ω Im $\sigma_{xy}(\omega)$ and Re $\sigma^{\uparrow}_{xx}(\omega)$, Re $\sigma^{\downarrow}_{xx}(\omega)$. We see from figures 1–5 that, at $0.5\ \mathrm{eV} \leqslant \hbar\omega < 4\ \mathrm{eV}$, Im $\sigma_{xy}(\omega)$ has features at the same frequencies as Re $\sigma^{\downarrow}_{xx}(\omega)$. This is a consequence of the nearly complete occupation of the spin-up valence band as was indicated above.

The negative peak in the ultraviolet region is also characteristic of the metals in question. Its origin can be explained as follows. We have already mentioned the two paired peaks of Re $\sigma_{xx}(\omega)$ at $\hbar\omega \simeq W_d$ produced by the transitions between the lower $1\uparrow, \downarrow$ and upper $6\uparrow, \downarrow$ valence sub-bands with the exchange splitting of the sixth band significantly greater than that of the first band. The same feature of the electron structure leads to the appearance of the typical zigzag on the curve Im $\sigma_{xy}(\omega)$ and to the change in its sign. The positive and negative pieces of the zigzag correspond to the spin-up and spin-down transitions, respectively. The interval between the point of the sign change and the negative peak on curve Im $\sigma_{xy}(\omega)$ corresponds approximately to half the exchange splitting Δ^{d}_{xc}. We can argue our conclusions using equations (10) and (11). At energies $\hbar\omega \geqslant W_d$ we can remove all bands from the summation over occupied bands m' in equation (10) keeping only $1\uparrow$ and $1\downarrow$ of sp type. Because the energy of interest is of the order of W_d, the main contributions come from the unoccupied states m near the top of d band. Hence, equation (10) can be written as follows:

$$\mathrm{Im}\ \sigma_{xy}(\omega) = \frac{\pi e^2}{\hbar\omega m^2} \sum_{kd' \neq d} F^{xy}_{sd}(\boldsymbol{k})\{\delta[\hbar\omega - E_{ds\uparrow}(\boldsymbol{k})]f_{ks\uparrow}(1 - f_{kd\uparrow}) - \delta[\hbar\omega - E_{ds\downarrow}(\boldsymbol{k})]f_{ks\downarrow}(1 - f_{kd\downarrow})\}. \tag{13}$$

It is clear from equation (13) that the curve Im $\sigma_{xy}(\omega)$ changes its sign at $\hbar\omega \simeq \frac{1}{2}\langle E_{ds\uparrow} + E_{ds\downarrow}\rangle$ and has two peaks of opposite signs at $\hbar\omega_1 = \langle E_{ds\uparrow}\rangle \simeq W_d$ and $\hbar\omega_2 = \langle E_{ds\downarrow}\rangle \simeq W_d + 2\Delta^{d}_{xc}$. Thus we come to the conclusion that the value of the exchange splitting can be directly extracted from the magneto-optical data.

There is rather good agreement between the calculated and experimental curves Im $\sigma_{xy}(\omega)$ for iron and cobalt. However, the nickel calculation of Im $\sigma_{xy}(\omega)$ is too broad by almost 40% (in energy scale) in comparison with experiment. A similar discrepancy was found between the band-structure calculations and the photoemission measurements [18]. Also there is some uncertainty concerning the value of the exchange splitting

of Ni. More detailed information about the theoretical and experimental values of W_d and $2\Delta_{xc}^d$ is presented in tables 1 and 2. For Ni the theoretical value of $2\Delta_{xc}^d$ is nearly twice that obtained from the photoemission data [19], but it is less than the value extracted from the magneto-optical measurements of Im $\sigma_{xy}(\omega)$. In principle such extraction is not very accurate because of the smoothness of experimental curves, on the one hand, and because of the deficit of experimental data for the ultraviolet region (for Fe and Co), on the other hand. In the other metals in question (Fe and Co), both W_d and $2\Delta_{xc}^d$ are in sufficiently good accordance with experiment. It should be noted that the above-mentioned discrepancies for Ni were widely discussed earlier in connection with the photoemission measurements (see, e.g., [20, 21]). Probably these difficulties are due to the inadequacy of the LSDA for the description of one-electron spectra which appears to be removed by accounting for the self-energy corrections.

4. Low-frequency behaviour of the conductivity tensor ($\hbar\omega \simeq 2\bar{\xi}$)

In the infrared region the analysis of the dynamical properties of the tensor $\sigma_{\alpha\beta}(\omega)$ is more complicated. Equation (10) is no longer valid at energies of the order of the SO splitting because it is incorrect in the vicinity of the degenerate state. So we also carried out an analysis of $\sigma_{\alpha\beta}(\omega)$ at $\hbar\omega \simeq 2\bar{\xi}$ taking into account the effect of a SO hybridisation. We begin this section with some formal expressions; then we continue by presenting results of numerical calculation and their comparison with experiments, for both optics and magneto-optics. A very fine k-mesh in the BZ is required for low frequencies in order to achieve higher accuracy. Such accuracy has been achieved by using a fine k-mesh for the BZ regions which are expected to give the main contribution, i.e. equivalent to the calculation with the total number of k-points of about 5000–10 000 over the whole irreducible part of BZ.

4.1. Analytical expressions for the usual optics

At first we consider the diagonal term Re $\sigma_{\alpha\alpha}(\omega)$. There are only three situations when a non-zero contribution to optical conductivity exists at small frequencies.

Situation I is when the non-relativistic bands with the same spin projection are degenerated or at least separated by not more than $2\bar{\xi}$.

Situation II is when the Fermi surface sheets with the opposite spin projections intersect.

Situation III is when there are nearly parallel Fermi surface sheets, corresponding to the spin-split bands (naturally with the opposite spin projections).

The presence of a SO coupling is not of importance for contribution of type I. In this case the influence of the SO coupling normally results in the removal of the degeneracy and in the appearance of the interband threshold at $\hbar\omega \leqslant 2\bar{\xi}$.

The mechanisms II and III appear only in the presence of the SO coupling because transitions between bands with opposite spins are otherwise forbidden.

The detailed study is based on the $\boldsymbol{k}\cdot\boldsymbol{p}$ perturbation theory and takes into account the interband hybridisation due to SO coupling [22]:

$$\psi_\gamma(\boldsymbol{r}) = c_{\gamma\uparrow}\,\psi_{m\uparrow}(\boldsymbol{r}) + c_{\gamma\downarrow}\,\psi_{m\downarrow}(\boldsymbol{r}) \qquad \gamma = 1, 2. \tag{14}$$

The expansion coefficients $c_{\gamma\sigma}$ are determined by the normalisation condition for the wavefunctions $\psi_\gamma(\boldsymbol{r})$ and by the equations

$$\begin{aligned}(E_{m\uparrow} + \langle \boldsymbol{k}m\uparrow|\hat{H}_{SO}|\boldsymbol{k}m\uparrow\rangle - E_\gamma)c_{\gamma\uparrow} + \langle \boldsymbol{k}m\uparrow|\hat{H}_{SO}|\boldsymbol{k}m'\downarrow\rangle c_{\gamma\downarrow} &= 0\\ \langle \boldsymbol{k}m'\downarrow|\hat{H}_{SO}|\boldsymbol{k}m\uparrow\rangle c_\gamma + (E_{m'\downarrow} + \langle \boldsymbol{k}m'\downarrow|\hat{H}_{SO}|\boldsymbol{k}m'\downarrow\rangle - E_\gamma)c_{\gamma\downarrow} &= 0\end{aligned} \tag{15}$$

where $\hat{H}_{SO} \equiv \xi(r)\hat{\boldsymbol{\sigma}}\cdot\hat{\boldsymbol{l}}$. The one-particle spectrum $E(\boldsymbol{k})$ is derived from equation (15):

$$E_\gamma(\boldsymbol{k}) = \tfrac{1}{2}(E_{m\uparrow} + E_{m'\downarrow}) \pm \sqrt{\tfrac{1}{4}(E_{m\uparrow} - E_{m'\downarrow})^2 + 4|\langle \boldsymbol{k}m\uparrow|\hat{H}_{SO}|\boldsymbol{k}m'\downarrow\rangle|^2}. \tag{16}$$

Substitution of equations (14) and (16) into equation (1) leads after some manipulations to the expression describing situation II:

$$\mathrm{Re}\,\sigma_{xx}^{II}(\omega) \simeq \frac{\pi e^2}{\hbar(2\pi)^3}\oint_L \frac{\mathrm{d}l_k\,|\xi_k|^2\theta(\hbar\omega - 2|\xi_k|)}{\hbar\omega\sqrt{\hbar^2\omega^2 - 4|\xi_k|^2}}\,\frac{|v_x^-(\boldsymbol{k})|^2}{\boldsymbol{v}^-(\boldsymbol{k})\times\boldsymbol{v}^+(\boldsymbol{k})} \tag{17}$$

where $\boldsymbol{v}^\pm(\boldsymbol{k}) \equiv \frac{1}{2}[\boldsymbol{v}_{m\uparrow}(\boldsymbol{k}) \pm \boldsymbol{v}_{m'\downarrow}(\boldsymbol{k})]$, $\xi_k \equiv \langle \boldsymbol{k}m\uparrow|\hat{H}_{SO}|\boldsymbol{k}m'\downarrow\rangle$, and the integral is taken along the line L of the intersection of the non-relativistic bands m and m'. Equation (17) gives rise to the sharp peak on the curve Re $\sigma_{xx}(\omega)$ at $\hbar\omega \simeq 2\bar{\xi}$ (if ξ_k does not depend on $\boldsymbol{k}$, then a square root singularity occurs) and falling as $1/\omega^2$ at higher energies.

In the same way we can get the following approximate expression for the conductivity in situation III:

$$\begin{aligned}\mathrm{Re}\,\sigma_{xx}^{III}(\omega) \simeq \frac{4\pi e^2}{\hbar(2\pi)^3}\oint\!\!\oint \mathrm{d}s_k\,\frac{|\xi_k|^2}{\hbar^2\omega^2}\left[1 + \frac{2\Delta_{xc}(\boldsymbol{k})}{\hbar\omega}\right]\\ \times\,\delta(\hbar\omega - 2\sqrt{\Delta_{xc}^2(\boldsymbol{k}) + |\xi_k|^2})\,\frac{|v_x^-(\boldsymbol{k})|^2}{|\boldsymbol{v}(\boldsymbol{k})|}\,\theta[\hbar\omega - 2\Delta_{xc}(\boldsymbol{k})]\end{aligned} \tag{18}$$

where $\Delta_{xc}(\boldsymbol{k}) \equiv \frac{1}{2}[E_{m\downarrow}(\boldsymbol{k}) - E_{m\uparrow}(\boldsymbol{k})]$, $v_x^- \equiv \frac{1}{2}[v_{m\uparrow x}(\boldsymbol{k}) \pm v_{m\downarrow x}(\boldsymbol{k})]$, $\xi_{\mathbf{k}} \equiv \langle \boldsymbol{k}m\uparrow|\hat{H}_{SO}|\boldsymbol{k}m\downarrow\rangle$. The integration in equation (18) is performed over those sections S of the Fermi surface, where bands $m\uparrow$ and $m\downarrow$ separated in energy by $2\Delta_{xc}(\boldsymbol{k})$ are nearly parallel. In the limit of small exchange splitting ($2\Delta_{xc}(\boldsymbol{k}) \simeq 2\bar{\xi}$) the ratios $\xi/\bar{\xi}$ and $v^-(\boldsymbol{k})/v(\boldsymbol{k})$ entering equation (18) are of the order of $\Delta_{xc}(\boldsymbol{k})/\Delta E$ (ΔE is the energy difference between $m\uparrow$ or $m\downarrow$ and the band nearest to them). Mechanism III is especially effective when the exchange splitting $2\Delta_{xc}(\boldsymbol{k})$ is considerably dispersive. This condition is satisfied when the bands $m\uparrow$ and $m\downarrow$ mentioned above are strongly hybridised with another band. If there is no dispersion of $\Delta_{xc}(\boldsymbol{k})$ then $v_x^- \simeq \partial[\Delta_{xc}(\boldsymbol{k})]/\partial\hbar k_x = 0$ and the effect disappears. Thus the main contribution is due either to situation II or to situation III depending on the relative magnitudes of the exchange and SO splitting. Situation II takes place in all metals with the magnetisation $\mu \simeq 1$. Situation III corresponds to a small magnetisation $\mu \ll 1$ and exchange splitting $2\Delta_{xc}(\boldsymbol{k}) \simeq 2\bar{\xi}$ at the Fermi level. In the case when $\Delta_{xc}(\boldsymbol{k}) \gg \bar{\xi}$ the total length of the intersection of Fermi surface sheets with the opposite spin projections is large enough that $(\bar{\xi}/\hbar v_F)\oint_L \mathrm{d}l_k/\oint\!\!\oint_S \mathrm{d}s_k \gg 1$. The transitions of type II are absent in this case and hence transitions of type II are dominant at $\hbar\omega \simeq \bar{\xi}$. In the case when $\Delta_{xc}(\boldsymbol{k}) \simeq \bar{\xi}$ at the Fermi

level, the total area of the Fermi surface sheets with opposite spins separated by exchange splitting $2\Delta_{xc}$ is of the same order as the Fermi surface area owing to the topological similarity of these sheets. So, in this case, $(\bar{\xi}/\hbar v_F) \oint_L dl_k / \oint\oint_S ds_k \ll 1$, i.e. transitions of type II are negligible. Moreover, when there is a band close to the $m\uparrow$ and/or $m\downarrow$ bands by $\Delta E \simeq \Delta_{xc}$, then the quantities contained in the integrated function in the right-hand side of equation (18) are of the same order as the similar quantities in equation (17). Therefore, when $\Delta_{xc} \simeq \bar{\xi}$ and there is a band near the $m\uparrow$ and $m\downarrow$ bands, the transition of type III prevails over all the others. At the same time, certain contributions of the usual type I can occur. However, these contributions do not have such sharp anomalies of the frequency dependence at $\hbar\omega \simeq 2\bar{\xi}$.

4.2. *Analytical expressions for magneto-optics*

In the infrared region at $\hbar\omega \simeq 2\bar{\xi}$ the main contributions to the non-diagonal term Im $\sigma_{xy}(\omega)$ can be classified in the same manner as for the diagonal term (situations I–III of section 4.1.). In distinction from the diagonal contributions we must take into account other than the SO hybridisation of the two given bands their hybridisation with other bands as well.

The expression for case I can be derived from equation (2) in the same manner as equation (10), but in view of the small energy difference $E_{mm'\sigma} \leqslant 2\bar{\xi}$ we must take into account the hybridisation between $m\sigma$ and $m'\sigma$ not to first order in ξ but exactly. It can be easily obtained for the given bands $m\sigma$ and $m'\sigma$ hybridised by a SO coupling that gives $(\hbar/a)^{-2}\,\mathrm{Im}[\langle m'|\hat{p}_x|m\rangle\langle m|\hat{p}_y|m'\rangle \simeq 1$ (a is the lattice parameter). The total contribution to Im $\sigma_{xy}(\omega)$ is proportional to the volume of $\boldsymbol{k}$-space regions where $E_{m\sigma}(\boldsymbol{k}) > E_F > E_{m'\sigma}(\boldsymbol{k})$ and $E_{m'\sigma}(\boldsymbol{k}) - E_{m\sigma}(\boldsymbol{k}) < 2\bar{\xi}$. Because of symmetry restrictions this contribution is zero for cubic metals but has a finite value for metals with the HCP structure:

$$\mathrm{Im}\,\sigma^{\mathrm{I}}_{xy}(\omega) = \frac{\pi e^2}{2\hbar^2\omega(2\pi)^3} \oint_L dk_z \frac{v_x^- v_y^{m\sigma,m'\sigma} - v_y^- v_x^{m\sigma,m'\sigma}}{|v_\perp \| v_z|} \times \mathrm{Im}\,\xi_k\, \theta(\hbar\omega - 2|\xi_k|). \tag{19}$$

In equation (19), $v_\perp(v_z)$ denotes components of the velocity normal (parallel) to the c axis in $\boldsymbol{k}$-space where the $m\sigma$- and $m'\sigma$-bands are degenerate, $\boldsymbol{v}^- \equiv \frac{1}{2}[\boldsymbol{v}_{m\sigma}(\boldsymbol{k}) - \boldsymbol{v}_{m'\sigma}(\boldsymbol{k})]$, $\xi_k \equiv \langle m\sigma|H_{SO}|m'\sigma\rangle$ and $\boldsymbol{v}^{m\sigma,m'\sigma} \equiv \langle m\sigma|\hat{\boldsymbol{p}}/m|m'\sigma\rangle$. The integration is performed over the line L where the $m\sigma$- and $m'\sigma$-bands are degenerate. Such lines for the HCP metals lie in the hexagonal plane of BZ [7].

The factors in the formulae for the diagonal component of the tensor are also typical for the non-diagonal component Im $\sigma_{xy}(\omega)$ in cases II and III. After some calculations we come to the following expression for Im $\sigma_{xy}(\omega)$ in case II:

$$\mathrm{Im}\,\sigma^{\mathrm{II}}_{xy}(\omega) \simeq \frac{8\pi e^2}{\hbar(2\pi)^3} \oint_L dl_k \frac{\theta(\hbar\omega - 2|\xi_k|)\,\mathrm{Im}\,\xi_k}{\hbar\omega\sqrt{\hbar^2\omega^2 - 4|\xi_k|^2}} \times {\sum_i}' \left[\left(\frac{\mathrm{Re}\,H_{SO}^{m'\downarrow,i\uparrow}}{E_{i\uparrow} - E_F} V_{xy}^{i\uparrow,m\uparrow} + \frac{\mathrm{Re}\,H_{SO}^{m\uparrow,i\downarrow}}{E_{i\downarrow} - E_F} V_{xy}^{i\downarrow,m'\downarrow} \right) \times \frac{|\xi_k|^2}{4\hbar\omega} + \left(\frac{\mathrm{Im}\,H_{SO}^{m\uparrow,i\uparrow}}{E_{i\uparrow} - E_F} V_{xy}^{i\uparrow,m\uparrow} + \frac{\mathrm{Im}\,H_{SO}^{m'\downarrow,i\downarrow}}{E_{i\downarrow} - E_F} V_{xy}^{i\downarrow,m'\downarrow} \right) \mathrm{Im}\,\xi_k \right] \tag{20}$$

where

$$V_{xy}^{i\sigma,j\sigma} \equiv (v_x^- v_y^{i\sigma,j\sigma} - v_y^- v_x^{i\sigma,j\sigma})/|\boldsymbol{v}^- \times \boldsymbol{v}^+| \qquad H_{SO}^{i\sigma,j\sigma} \equiv \langle ki\sigma|\hat{H}_{SO}|kj\sigma'\rangle.$$

The notation equation in (20) is the same as in equation (17). It is obviously seen that Im $\sigma_{xy}(\omega)$ is antisymmetric with respect to the transposition $x \rightleftarrows y$. As was mentioned above, the derivation of equation (20) requires taking into account both the SO hybridisation of the $m\uparrow$ - and $m'\downarrow$ -bands with opposite spins and the admixture of other bands $i\sigma$ to $m\uparrow$, $m'\downarrow$ owing to the SO coupling. Note that the contribution (20) is smaller than the similar contribution to diagonal component Re $\sigma_{xx}(\omega)$ by the factor $\bar{\xi}/\overline{\Delta E_{\lambda\lambda'}}$.

If we include the SO hybridisation of the nearly parallel bands with opposite spins in our calculations, then we shall obtain the contribution in Im $\sigma_{xy}(\omega)$ describing case III:

$$\begin{aligned}\operatorname{Im}\sigma_{xy}^{\mathrm{III}}(\omega) \simeq -\frac{8\pi e^2}{\hbar(2\pi)^3}\oint\!\!\oint_S \mathrm{d}s_k\,\delta(\hbar\omega - 2\sqrt{\Delta_{xc}^2 + |\xi_k|^2})\,\theta(\hbar\omega - 2\Delta_{xc})\frac{\operatorname{Im}\xi_k}{\hbar\omega}\\ \times \sum_i{}' \left[\left(\frac{\operatorname{Re} H_{SO}^{m'\downarrow,i\uparrow}}{E_{i\uparrow} - E_F} W_{xy}^{i\uparrow,m\uparrow} + \frac{\operatorname{Re} H_{SO}^{m\uparrow,i\downarrow}}{E_{i\downarrow} - E_F} W_{xy}^{i\downarrow,m'\downarrow}\right)\frac{|\xi_k|^2}{4\hbar^2\omega^2}\right.\\ \left. + \left(\frac{\operatorname{Im} H_{SO}^{m\uparrow,i\uparrow}}{E_{i\uparrow} - E_F} W_{xy}^{i\uparrow,m\uparrow} + \frac{\operatorname{Im} H_{SO}^{m'\downarrow,i\downarrow}}{E_{i\downarrow} - E_F} W_{xy}^{i\downarrow,m'\downarrow}\right)\frac{2\operatorname{Im}\xi_k}{\hbar\omega}\left(1 + \frac{2\Delta_{xc}}{\hbar\omega}\right)\right]\end{aligned} \tag{21}$$

where

$$V_{xy}^{i\sigma,j\sigma} \equiv (v_x^- v_y^{i\sigma,j\sigma} - v_y^- v_x^{i\sigma,j\sigma})/|\boldsymbol{v}_k|.$$

The integration in equation (21) is performed over the same surface S as in equation (18). As follows from equation (21) there is the anomaly of Im $\sigma_{xy}(\omega)$ at $\hbar\omega = 2\sqrt{\Delta_{xc}^2 + |\bar{\xi}|^2}$ (Δ_{xc} is the exchange splitting at the Fermi level: $2\Delta_{xc} \ll \overline{\Delta E_{\lambda\lambda}}$).

4.3. Numerical calculations; comparison with experiment

As was discussed above, there are certain mechanisms playing a dominant role in the formation of $\sigma_{\alpha\beta}(\omega)$ in the infrared region. Their occurrence depends on the value of the spin moment μ. In the case of Fe and Co where the spin moment is relatively large, the main contribution to $\sigma_{\alpha\beta}(\omega)$ comes from the interband transitions in the vicinity of the crossing of bands with opposite spins (mechanism II). It is easily seen from figure 7(*a*), that for Fe such a manifold in $\boldsymbol{k}$-space consists of the intersections of the electron spheres with an H-centred octahedron. The interband transitions in this manifold cause the anomaly of Re $\sigma_{xx}(\omega)$ and Im $\sigma_{xy}(\omega)$ at $\hbar\omega \simeq 2\bar{\xi}$, and that at $\hbar\omega \simeq 0.15$ eV for Fe in accordance with experiment [15]. An anomaly of the same nature takes place at $\hbar\omega \simeq 0.19$ eV for FCC Co. The calculations for Co in the infrared region were carried out only for the FCC phase because of the time limitation but this anomaly can be related to the rather sharp structure observed in experiment [17] for HCP Co when it is considered that mechanism II is not sensitive to crystal structure. The curves Re $\sigma_{xx}(\omega)$ for Fe, Co and Ni are presented in figure 8. That the effect of the SO coupling is responsible for the anomaly is seen from figure 8, where one of the calculated curves is obtained by including this effect, and the other is obtained without including this effect. Furthermore, to be convinced that the hybridisation between bands with the opposite spins by means of SO coupling is the cause of the anomaly in question, we carried out the calculations of Re $\sigma_{xx}(\omega)$, excluding from the LMTO Hamiltonian matrix the indicated terms responsible for hybridisation. The anomaly disappears, as is seen from figure 9(*a*).

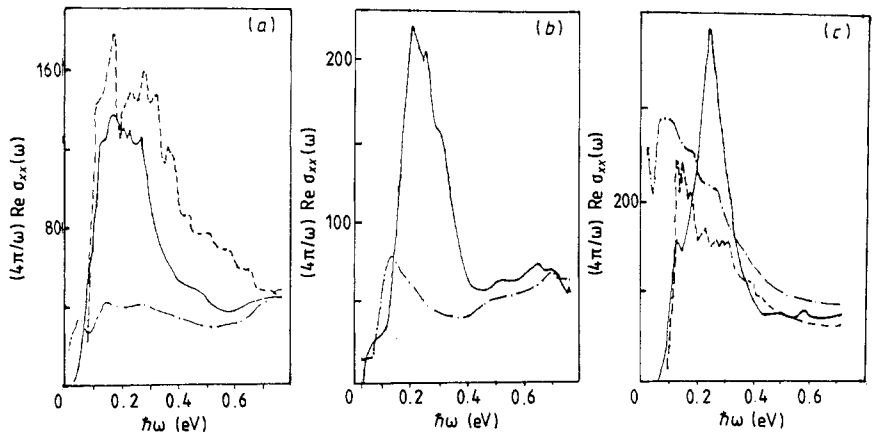

Figure 8. Frequency dependence of $(4\pi/\omega)$ Re $\sigma_{xx}(\omega)$ in the infrared region (*a*) for Fe, (*b*) for Co and (*c*) for Ni: ——, with SO effect; — · —, without SO effect; – – –, experiment (for Fe), [15] and for Ni [16].

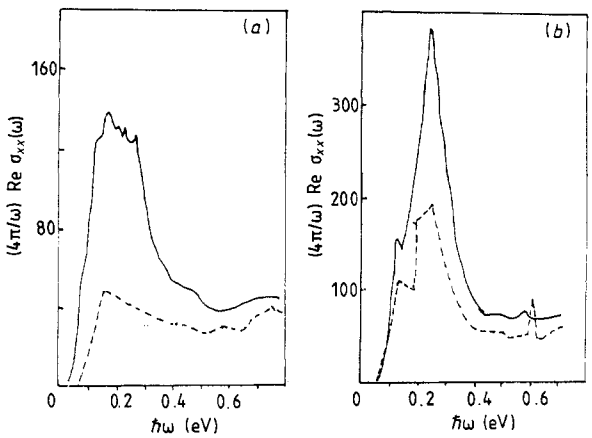

Figure 9. Illustration of the dominant role of the SO hybridisation of sub-bands with the opposite spins by the picture of the conductivity tensor anomalies at $\hbar\omega \simeq 2\bar{\xi}$ (or $2\sqrt{\Delta^2 + \bar{\xi}^2}$ for (*a*) Fe and (*b*) Ni: ——, inclusion of the full LMTO Hamiltonian matrix; – – –, exclusion of the terms describing the hybridisation with the opposite spins in the LMTO Hamiltonian matrix.

The conductivity of Ni has a similar peak at $\hbar\omega \simeq 2\sqrt{\Delta_{xc}^2 + |\bar{\xi}|^2}$ but its origin is of another type corresponding to the relatively small value of the exchange splitting $2\Delta_{xc} \simeq 2\bar{\xi}$ and of the spin moment $\mu = 0.55\mu_B$. As is seen from figure 7(*b*) in this case the intersections of the Fermi surface sheets are small, but in accordance with the discussions in sections 4.1 and 4.2 the contributions to the conductivity tensor are due to the transitions between the exchange-split bands (namely $6\uparrow$ and $6\downarrow$) separated by nearly $2\sqrt{\Delta_{xc}^2 + |\bar{\xi}|^2}$ (mechanism III). As a result these transitions occur in a $\boldsymbol{k}$-space region enclosed between the sheets $e_{6\uparrow}$ and $e_{6\downarrow}$ and cause the anomaly of Re $\sigma_{xx}(\omega)$ and Im $\sigma_{xy}(\omega)$ at $\hbar\omega \simeq 0.26$ eV (figures 8 and 10). The experimental curve has a similar feature at $\hbar\omega \simeq 0.28$ eV [23] and at $\hbar\omega \simeq 0.30$ eV [9]. One can conclude that $2\Delta_{xc} \simeq 0.24$ eV at the Fermi level assuming that $2\bar{\xi} = 0.18$ eV. To be convinced that mechanism III is responsible for the anomaly in question we also calculated Re $\sigma_{xx}(\omega)$ for Ni in the same manner as for Fe, neglecting only the hybridisation between bands with the

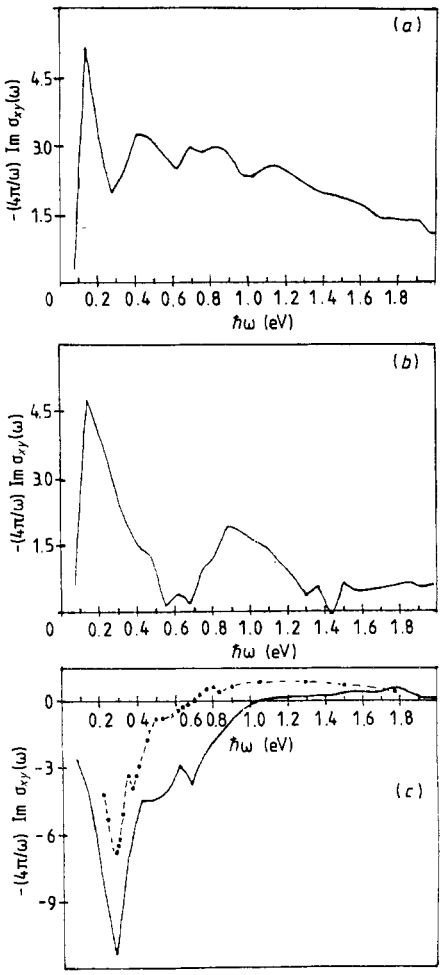

Figure 10. Frequency dependence of $(-4\pi/\omega)$ Im $\sigma_{xy}(\omega)$ in the infrared region (*a*) for Fe, (*b*) for Co and (*c*) for Ni: – – ● – –, experiment [10].

opposite spins. Then this peak decreases significantly (see figure 9(*b*)). Thus these results confirm that mechanism III is responsible for the anomaly indicated in Ni.

In Ni the curve Re $\sigma_{xx}(\omega)$ has the peak at $\hbar\omega = 0.75$ eV which is produced by the spin-down transitions mainly in the vicinity of Γ–K and Γ–W directions. The spin-up transitions are entirely absent at $\hbar\omega < 0.5$ eV because of the very low density of spin-up states at the Fermi level. Thus, if we take into account that $\mathrm{Re}[\sigma_{xx}^{\downarrow}(\omega) - \sigma_{xx}^{\uparrow}(\omega)] \simeq \mathrm{Re}\,\sigma_{xx}^{\downarrow}(\omega)$ owing to the threshold of spin-up transitions just mentioned, the presence of the negative peak of Im $\sigma_{xy}(\omega)$ at $\hbar\omega = 0.75$ eV will be quite clear. The experimental curve Im $\sigma_{xy}(\omega)$ has a small height at the same energy.

Besides the anomalous contributions there are also the usual ones (of type I) in $\sigma_{\alpha\beta}(\omega)$ at $\hbar\omega \simeq 2\tilde{\xi}$ having a monotonic frequency dependence. In iron these transitions occur in the neighbourhood of point H, and in nickel mainly in the Γ–U direction.

5. Conclusions

The optical and magneto-optical properties of Fe, Co and Ni have been studied by using LSDA one-particle spectra. In accordance with our analysis given in the present work it

is possible to extract information about the electron and especially about the spin structure of the ferromagnetic metals. It follows both from the analytical consideration and from the numerical calculations that the magnetic ordering and the relativistic effects show up in magneto-optics as in usual optics. However, the non-diagonal components $\sigma_{\alpha\beta}$ ($\alpha \neq \beta$) reproduce the magnetic and relativistic effects more distinctly than diagonal components because magnetism and SO coupling are the basis of MO effects.

We specifically suggested a number of the interband transition mechanisms playing a dominant role in the formation of $\sigma_{\alpha\beta}(\omega)$ in the infrared region. All mechanisms lead to the appearance of $\sigma_{\alpha\beta}(\omega)$ features at $\hbar\omega \simeq 2\bar{\xi}$ and hence their arbitrary combinations allow us to determine a SO coupling value from the optical and magneto-optical curves. These mechanisms are of a universal type and we predict that they occur not only in 3D ferromagnets but also in compounds and other metals. The specific behaviour of Im $\sigma_{xy}(\omega)$ at $\hbar\omega \simeq W_d$ which is accompanied by the change in its sign is peculiar to 3D metals on the one hand and can be manifested in any form in other ferromagnetic metals and compounds on the other hand.

We believe that our work will be useful in the treatment of optical and magneto-optical properties of either metals and compounds.

Acknowledgments

The authors would like to express their thanks to Professor G S Krinchik and Dr E A Gan'shina for valuable discussions. One of us (YuU) is grateful to Professor O K Andersen for his interest in our work and his hospitality at the Max-Planck Institut.

References

[1] Singh M, Wang C S and Callaway J 1975 *Phys. Rev.* B **11** 287
[2] Wang C S and Callaway J 1974 *Phys. Rev.* B **9** 4897
[3] Ebert E, Strange P and Gyorffy B L 1989 *J. Physique Coll.* **49** 31
[4] Debnath N C, Chowdhuri M and Chatterjee S 1985 *J. Phys. F: Met. Phys.* **15** 1693
[5] Callaway J and Wang C S 1977 *Phys. Rev.* B **16** 2095
[6] Rashkeev S N, Uspenskii Yu A and Mazin I I 1985 *Zh. Eksp. Teor. Fiz.* **88** 1687
[7] Kubo R 1957 *J. Phys. Soc. Japan* **12** 570
[8] Kleiner W H 1966 *Phys. Rev.* **142** 318
[9] Johnson P B and Christy R W 1974 *Phys. Rev.* B **9** 5056
[10] Krinchik G S and Artem'ev V A 1967 *Zh. Exp. Teor. Fiz.* **53** 1901
[11] Krinchik G S and Gan'shina E A 1973 *Zh. Exp. Teor. Fiz.* **65** 1970
[12] Argyres P N 1955 *Phys. Rev.* **97** 334
[13] Andersen O K 1975 *Phys. Rev.* B **12** 3060
[14] Uspenskii Yu A, Maksimov E G, Mazin I I and Rashkeev S N 1983 *Z. Phys.* **53** 263
[15] Shirokovskii V P, Kirillova M M and Shilkova N A 1982 *Zh. Exp. Teor. Fiz.* **82** 784
[16] Kirillova M M 1971 *Zh. Exp. Teor. Fiz.* **61** 336
[17] Kirillova M M, Bolotin G A and Nomerovannaya L V 1980 *Opt. Spectrosc.* **49** 742
[18] Eastman D E, Himpsel F J and Knapp J A 1978 *Phys. Rev. Lett.* **40** 1514
[19] Maetz C S, Gerhardt U, Dietz E, Ziegler A and Jelitto R J 1982 *Phys. Rev. Lett.* **48** 1686
[20] Liebsch A 1981 *Phys. Rev.* B **23** 5203
[21] Smith N V, Lasser R and Chiang S 1982 *Phys. Rev.* B **25** 793
[22] Halilov S V, Rajkeev S N and Uspenskii Yu A 1987 *Fiz. Tverd. Tela* **29** 1467
[23] Krinchik G S and Nurmukhamedov G M 1965 *Zh. Exp. Teor. Fiz.* **48** 34
[24] Pessa M, Heimann P and Neddermeyer H 1976 *Phys. Rev.* B **14** 3488
[25] Himpsel F J and Eastman D E 1980 *Phys. Rev.* B **21** 3207

[26] Feder R, Gudat U, Kisker E, Rodriguez A and Schroder K 1983 *Solid State Commun.* **46** 619
[27] Eastman D E, Himpsel F J and Knapp J A 1980 *Phys. Rev. Lett.* **44** 95
[28] Heimann P, Himpsel F J and Eastman D E 1981 *Solid State Commun.* **39** 219